Flight Control Reconfiguration in Oscillatory Failure Case Scenarios

Daniel Ossmann [*] **Christian Weiser** [**] **Felix Biertümpfel** [***]
Harald Pfifer [***] **Jérôme Cieslak** [****]

[*] *Munich University of Applied Sciences HM, 80335 Munich, Germany (e-mail: daniel.ossmann@hm.edu)*
[**] *Institute of System Dynamics & Control, DLR, 82234 Wessling, Germany (e-mail: christian.weiser@dlr.de)*
[***] *Chair of Flight Mechanics & Control, TU Dresden, 01069 Dresden, Germany (e-mail: {harald.pfifer, felix.biertuempfel}@tu-dresden.de)*
[****] *Univ. Bordeaux, CNRS, Bordeaux INP, IMS, UMR 5218, F-33400 Talence, France (e-mail: jerome.cieslak@ims-bordeaux.fr)*

Abstract: A fault detection system together with a flight control reconfiguration algorithm is proposed to tackle the problem of oscillatory failure case scenarios in hydraulically actuated flight control loops. The fault detection system employs a set of residual filters designed using a model-based approach via command-input decoupling and free assignment of the filter dynamics via dynamic inversion. As underlying design model, an optimized, multi-model hydraulic actuator approximation covering the actuator dynamics together with stochastically distributed, uncertain parameters is derived. A flight control reconfiguration algorithm is presented which smoothly transitions the control law from its normal configuration to the alternate law after detection of a fault. The performance of the transition is analyzed using advanced linear time-varying analysis methods based on an extension of the well-known Bounded Real Lemma. The achieved detection and reconfiguration performance is verified via non-linear simulations.

Keywords: Fault tolerant control; Fault detection & diagnosis; Robust control; Aircraft control.

1. INTRODUCTION

The detection of failures and the subsequent reconfiguration of the flight control systems (FCS) is an important feature to be considered in today's aircraft design in order to increase aircraft autonomy and maintain optimal aircraft performance. One example of a failure influencing the aircraft performance and impacting the design process is the *oscillatory failure case* (OFC) in hydraulic actuators, see Goupil (2010). The early detection of an OFC allowing for FCS reconfiguration measures is important as a fully developed OFC can negatively affect not only the quality of the airplane's closed-loop response, i.e., the rigid body dynamics, but can also excite structural wing modes. This paper explicitly tackles the challenges described in the *Industrial Benchmark on Fault Detection and Fault Tolerant Control* dedicated to OFC detection and FCS reconfiguration provided as design challenge for the 2023 IFAC world congress, see Engelbrecht et al. (2022).The proposed solution to these challenges, which are summarized in Section 2, is a fault detection system triggering a flight control reconfiguration in case of the detection of an OFC. The fundamentals of the employed methods are summarized in Section 3.

The fault detection challenge for OFCs is the necessity of an early detection with a typical required detection time below three oscillation periods (Goupil (2010)) together with the necessity of detecting the smallest oscillation amplitudes possible. Limiting factors on the latter are measurement noise and turbulence acting on the aircraft. To address these fault detection challenges, a multi-model approximation of the actuator dynamics is developed. This approximation is necessary as not all parameters and inputs of the actuator are available online. For example, the aerodynamic force component acting on the actuator rod and the available hydraulic pressure delivered to the actuator are not fully known. This multi-model description of the actuator dynamics sets the basis for the model-based residual filter design described in Section 4. The design strategy employs command-input decoupling and free assignment of the filter dynamics via dynamic inversion to create a set of residual filters allowing a fast and robust OFC detection.

After the detection of an OFC, a controller reconfiguration and control input re-allocation algorithm (Section 5) ensures smooth transitions to the alternate control law. A common strategy after the OFC detection is to set the faulty actuator passive and to reconfigure to an alternate flight control law. For the design of the reconfiguration, the static and dynamic part of the alternate control law are separated to enable a hybrid switching scheme. The static part is reconfigured by a simple blending techniques, while the dynamic part is reconfigured using a bumpless scheme based on solving an algebraic Riccati equation. This approach enables an adequate update of the dynamic controller part of the alternate law as long as it is running off-line, i.e., in parallel mode. The closed-loop performance

of the transition is analyzed using advanced linear time-varying analysis methods based on an extension of the well-known Bounded Real Lemma. This analysis allows verifying efficiently the stability and performance without performing extensive non-linear simulation studies. Finally, the achieved closed-loop detection and reconfiguration performance is verified via non-linear simulations.

2. PROBLEM SETUP

As described in Engelbrecht et al. (2022) the OFC is occurring on one of two actuator-driven control surfaces steering the longitudinal motion of an aircraft. Thus, the available aircraft model describes the longitudinal aircraft behavior in cruise condition on a single trim-point. It is of fourth order, including pitch rate q, velocity V, angle of attack α, and pitch angle Θ. Measured outputs are pitch rate, load-factor n_z, and flight-path angle γ. The model's inputs are the elevator deflections δ, provided by two identical hydraulic actuators, and a disturbance input on the aircraft states to enable turbulence injection. The aircraft is augmented with the normal or the alternate control law, i.e., a downgraded control algorithm used in fault scenarios, see Engelbrecht et al. (2022); Ossmann et al. (2017). Both laws have the form

$$\begin{aligned} \dot{\xi} &= 0 \cdot \xi + [-k_i \;\; 0 \;\; k_i]\, u_c \\ \delta_c &= \xi + [k_f \;\; k_q \;\; k_{n_z}]\, u_c, \end{aligned} \tag{1}$$

where δ_c is the commanded elevator surface position, ξ and $\dot{\xi}$ are the controller state and its derivative, and $u_c = [n_{z,c}\; q\; n_z]^T$ is the controller input vector with the commanded load-factor $n_{z,c}$. $n_{z,c}$ is either provided by the pilot or by an outer control loop, i.e., a proportional γ-feedback. This outer loop is active when no pilot commands are provided to hold the aircraft in cruise condition. The gains k_{n_z} and k_q are the feedback gains on the load-factor and the pitch rate, k_i is the integral gain on the load-factor control error $e_{n_z} = n_z - n_{z,c}$, and k_f is the load-factor feed-forward gain. Subsequently, the integral gains are summarized by $\bar{k}_i := [-k_i\, 0\, k_i]$ and the proportional gains by $\bar{k}_p := [k_f\, k_q\, k_{n_z}]$. The position and rate limited command input δ_c is converted to a actuator rod position command x_c via a non-linear function and sent to the actuators. While normal and alternate law feature the exact same structure, the gains of the alternate law ($\bar{k}_p^{(\mathrm{alt})}$ and $\bar{k}_i^{(\mathrm{alt})}$) are lower, see Engelbrecht et al. (2022).

2.1 Actuator Model with Faults

Hydraulic actuators steer the two elevators. Each actuator features a proportional, rod position feedback loop to compute the servo-valve current. A non-linear first order actuator model is given by

$$\begin{aligned} \dot{x} &= v_c \sqrt{\frac{\Delta P^{\Delta} - F_A(x,\dot{x})/S}{\Delta P_r + k_d^{\Delta}\dot{x}^2/S}} \\ x_m &= x + n, \end{aligned} \tag{2}$$

where x and $\dot{x}$ is the rod position and velocity, respectively, x_m the measured rod position, n the sensor noise, ΔP the hydraulic differential pressure delivered to the actuator, ΔP_r the reference differential pressure, S the piston surface area and v_c the commanded rod velocity. The commanded velocity results from a non-linear mapping of the commanded current i_c by the servo controller, i.e., $v_c = f_{i_c \to v_c}(i_c)$. The servo controller generates the current from the error between the commanded rod position x_c and the measured rod position multiplied with the proportional gain k_p, i.e., $i_c = k_p(x_c - x_m)$. In equation (2), k_d is the damping coefficient and F_A is the aerodynamic force component acting on the actuator rod. The commanded and measured rod position are available in the FCS. The parameters ΔP_r and S can be assumed to be known and constant, while for the differential pressure ΔP and the damping coefficient k_d only the parameter range is known. These two parameters are uniformly distributed, which is indicated by "Δ" in (2). The aerodynamic force is a typical unknown disturbance to the actuator. The actuator rod position x and the control surface position δ are connected via a non-linear mapping $f_{x\to\delta}$. Thus, the commanded surface position δ_c in (1) is converted to the commanded rod position x_c via the inverse of this mapping, i.e., $f_{\delta_c \to x_c} = f_{x\to\delta}^{-1}$.

The OFC is defined by $f = A_f \cos(\omega_f)$, where A_f is the amplitude, ω_f the frequency, lying between 1 Hz and 10 Hz. The OFC is either injected to the measured rod position, mimicking a sensor fault in the servo loop, or to the current command i_c, mimicking a fault in the electro-hydraulic hardware cycle, see Engelbrecht et al. (2022). For both locations the OFC is modeled either as additive ("liquid") fault or as substituting ("solid") fault, completely replacing the actual signal.

2.2 The Challenge

The FCS extensions shall provide fast detections of small actuator OFCs and smooth controller reconfigurations. *Smooth* relates to no discontinuous FCS signals and no departures from the current flight state (Engelbrecht et al. (2022)). In addition, the alternate control law shall provide a similar closed-loop performance as it provides with two actuators available. Thus, in case of an actuator OFC the following three actions need to be taken: (i) detection of the OFC; (ii) smoothly deactivating the faulty actuator and reallocating the control input to the healthy actuator; (iii) smoothly activate the alternate control law.

3. THEORETICAL BACKGROUND

This section provides the theoretical background of the employed methods in this paper.

3.1 Model-Detection based Fault Detection

A model-based fault detection approach requires a design model of the underlying process to be monitored. Such a model must contain only known quantities. This is not the case for the actuator model described in Section 2.1, which includes randomly distributed parameters and an unknown force. To solve this problem, an approach based on the model-detection problem (Varga (2017)) is modified to solve the fault detection problem herein. For each model with fixed parameters, a residual filter is designed and the resulting residual vector is fused to a scalar residual. To describe the principal idea and shorten notation, the approach is presented for a linear system and extended to the non-linear actuator model in the application section. Generally, a residual filter processes known system outputs $y(t)$ and inputs $u(t)$ to generate the residual $r(t)$, which is decoupled from any inputs but the fault. Assume a linear multi-model system description of the form

$$y^{(i)}(s) = G_u^{(i)}(s)u(s) + G_d^{(i)}(s)d(s) + G_f^{(i)}(s)f(s), \tag{3}$$

where $y^{(i)}(s)$, $u(s)$, $d(s)$ and $f(s)$ are Laplace-transformed vectors of the output vector $y^{(i)}(t) \in \mathbb{R}^p$, the control input vector $u(t) \in \mathbb{R}^{m_u}$, the disturbance input vector $d(t) \in \mathbb{R}^{m_d}$, and the fault input vector $f(t) \in \mathbb{R}^{m_f}$. $G_u^{(i)}(s)$, $G_d^{(i)}(s)$ and $G_f^{(i)}(s)$ are the transfer function matrices from the control inputs to outputs, disturbance inputs to outputs and fault inputs to outputs, respectively, of the $i = 1, \ldots, M$ model. A residual filter for the i^{th} model is expressed by

$$r^{(i)}(s) = Q^{(i)}(s) \begin{bmatrix} y^{(i)}(s) \\ u(s) \end{bmatrix}. \tag{4}$$

Replacing $y^{(i)}(s)$ in (4) by (3) yields

$$r^{(i)}(s) = Q^{(i)}(s) \begin{bmatrix} G_u^{(i)}(s) & G_d^{(i)}(s) & G_f^{(i)}(s) \\ I & 0 & 0 \end{bmatrix} \begin{bmatrix} u(s) \\ d(s) \\ f(s) \end{bmatrix}. \tag{5}$$

To solve the fault detection problem for the i^{th} model, the choice of $Q^{(i)}(s)$ needs to guarantee the decoupling of all control and disturbance inputs from the residual $r^{(i)}$, i.e.,

$$Q^{(i)}(s) \begin{bmatrix} G_u^{(i)}(s) & G_d^{(i)}(s) \\ I & 0 \end{bmatrix} = 0, \tag{6}$$

and guarantee the coupling of the fault to the residual, i.e.,

$$Q^{(i)}(s) \begin{bmatrix} G_f^{(i)}(s) \\ 0 \end{bmatrix} \neq 0. \tag{7}$$

As additional constraint, the residual filter $Q^{(i)}(s)$ needs to be *stable* and *proper*. This formulation of the fault detection problem can be solved numerically for each i^{th} model using tools provided in Varga (2017). For the benchmark problem herein it is solved analytically.

As in the solution of the model detection problem, for the i^{th} filter $Q^{(i)}(s)$ the decoupling condition (6) for all other systems $j \neq i$ does not hold. However, in case the structure of $G_f^{(j)}(s)$ is constant over all M models, it can be assumed that the coupling condition (7) holds also $\forall j$. Then, a valid scalar residual can be computed online via

$$\hat{r}(t_k) = \min_i |r^{(i)}(t_k)|. \tag{8}$$

To generate the fault indicator i_f, the residual $\hat{r}$ is compared to a threshold τ in each time step, i.e.,

$$i_f(t_k) = \begin{cases} 0 & \text{if } \hat{r}(t_k) < \tau \\ 1 & \text{otherwise.} \end{cases} \tag{9}$$

3.2 Hybrid Bumpless Switching

A hybrid switching solution is proposed to maintain the given controller gains (Engelbrecht et al. (2022)) but mitigate reconfiguration transients. The static contribution $\delta_c^{(\text{p})}$, composed by the proportional gains ($\bar{k}_p$ and $\bar{k}_p^{(\text{alt})}$), is computed by a blending scheme. The dynamical (integral) contribution $\delta_c^{(\text{i})}$, composed by the integral gains ($\bar{k}_i$ and $\bar{k}_i^{(\text{alt})}$), is driven by a bumpless scheme following Turner and Walker (2000). The scheme originates from linear quadratic approaches to derive an optimal controller update matrix via solving an algebraic Riccati equation. The approach has been successfully applied in aerospace, see Cieslak et al. (2008, 2015). Finally, the control signal applied to the actuators is computed by $\delta_c = \delta_c^{(\text{p})} + \delta_c^{(\text{i})}$.

Blended scheme: let the fault indicator i_f defined in (9) be used to engage a smooth reconfiguration. The control signal $\delta_c^{(\text{p})}$ of the static part is determined by

$$\delta_c^{(\text{p})} = (Ts + 1)^{-1}((1 - i_f)\bar{k}_p + i_f \bar{k}_p^{(\text{alt})})u_c, \tag{10}$$

where the time constant T of the filter is set to achieve a smooth reconfiguration transients.

Bumpless scheme: before detection ($i_f = 0$) the integral part $\dot{\xi}^{(\text{alt})}$ of the alternate law according to (1) is extended by

$$\begin{aligned} &\text{on-line normal law} &&: \dot{\xi} = \bar{k}_i u_c \\ &\text{off-line alternate law} &&: \dot{\xi}^{(\text{alt})} = \bar{k}_i^{(\text{alt})} \alpha \end{aligned} \tag{11}$$

with $\alpha = F[\xi \ \xi^{(\text{alt})} \ u_c^T]^T$ and ξ and $\xi^{(\text{alt})}$ being the state of normal and the alternate law, respectively. F is a static matrix to be designed such that the quadratic cost function

$$J = \frac{1}{2} \int_0^\infty (z_u^T W_u z_u + z_\sigma^T W_\sigma z_\sigma) \text{dt} \tag{12}$$

is minimized, with $z_u = \xi^{(\text{alt})} - \xi$ and $z_\sigma = \alpha - u_c$. W_u and W_σ are constant positive-definite weighting matrices to determine the desired objectives. According to Turner and Walker (2000) the solution is given by

$$F = \Omega \, [F_1 \ F_2 \ F_3] \tag{13}$$

with

$$\begin{aligned} F_1 &= (\tilde{B}^T \Pi + \tilde{D}^T W_u \tilde{C})^T \\ F_2 &= (-\tilde{D}^T W_u + \tilde{B}^T M \cdot \\ &\quad (\tilde{C}^T W_u + \tilde{C}^T W_u \tilde{D} \Omega \tilde{D}^T + \Pi \tilde{B} \Omega \tilde{D} W_u))^T \\ F_3 &= (-W_\sigma + \tilde{B}^T M (\tilde{C}^T W_u \tilde{D} \Omega W_\sigma + \Pi \tilde{B} \Omega W_\sigma))^T \end{aligned} \tag{14}$$

The matrices $\tilde{A}$, $\tilde{B}$, $\tilde{C}$ and $\tilde{D}$ are the state-space matrices of the dynamical part of the alternate control law, $M = (\mathbf{A}^T + \Pi \mathbf{B})^{-1}$ and $\Omega = -(\tilde{D}^T W_u \tilde{D} + W_\sigma)^{-1}$. The matrix Π is the definite-positive solution of the algebraic Riccati equation

$$\Pi \mathbf{A} + \mathbf{A}^T \Pi + \Pi \mathbf{B} \Pi + \mathbf{C} = 0 \tag{15}$$

with $\mathbf{A} = \tilde{A} + \tilde{B} \Omega \tilde{D}^T W_u \tilde{C}$, $\mathbf{B} = \tilde{B} \Omega \tilde{B}^T$ and $\mathbf{C} = \tilde{C}^T W_u (1 + \tilde{D} \Omega \tilde{D}^T W_u) \tilde{C}$.

The presented approach enables a bumpless transfer via updating the alternate law's integrator running offline. When the reconfiguration is triggered, the integral contribution $\delta_c^{(\text{i})}$ can be switched directly from the normal law's contribution $\bar{k}_i u_c$ to the alternate law's contribution $\bar{k}_i^{(\text{alt})} u_c$.

3.3 Linear Time-Variant System Analysis

The reconfiguration is a time-variant process that can be analyzed efficiently using linear time-variant (LTV) techniques. They allow a rapid computation of the worst-case scenarios that can occur during the reconfiguration process, see Tadmor (1990); Biertümpfel and Pfifer (2022).

A finite horizon LTV system G is defined as

$$\begin{aligned} \dot{x}_t(t) &= A_G(t) \, x_G(t) + B_G(t) \, d(t) \\ e(t) &= C_G(t) \, x_G(t) + D_G(t) \, d(t), \end{aligned} \tag{16}$$

where $x_G(t) \in \mathbb{R}^{n_{x_t}}$ denotes the state vector, $d(t) \in \mathbb{R}^{n_d}$ the input vector, and $e(t) \in \mathbb{R}^{n_e}$ the performance output vector. Its system matrices are locally bounded continuous functions of time t and compatible size-wise to the corresponding vectors, e.g., $A_G(t) \in \mathbb{R}^{n_{x_G} \times n_{x_G}}$. The

upper bound on worst-case performance outputs at the end of the trajectory can be quantified by finite horizon energy-to-Euclidean gain. Assuming $D_G(t) = 0$, it is defined as (e.g. Tadmor (1990)):

$$\|G\|_{E[0,T]} = \sup_{\substack{d\in L_2[0,T] \\ d\neq 0, x(0)=0}} \frac{\|e(T)\|}{\|d(t)\|_{2[0,T]}}, \tag{17}$$

with

$$\|d\|_{2[0,T]} = \sqrt{\int_0^T d(t)^T d(t)\, dt} \tag{18}$$

describing the finite horizon Lebesgue 2-norm $L_2[0,T]$ of the signal $d(t)$. Consequently, this worst-case gain describes the ball upper bounding the performance output over all valid disturbance input signals in $L_2[0,T]$ at the final point of the trajectory. The restriction $D_G(t) = 0$, guarantees that the gain is well-defined. Note that the gain only upper bounds the output at the final time T. An analysis condition to upper bound $\|G\|_{E[0,T]}$ is based on the extension of the LTI Bounded Real Lemma to finite horizon LTV systems in Green and Limebeer (1995). The explicit formulation for (17) is given in Theorem 1.

Theorem 1. Let G be an LTV system defined by (16). Given $x(0) = 0$, if there exists a time-dependent, continuous differentiable symmetric matrix valued function $P : \mathbb{R}_0^+ \to \mathbb{R}^{n_x \times n_x}$ such that

$$P(T) = C_G(T)^T C_G(T) \tag{19}$$

and

$$\begin{aligned} \dot{P} = &- PA_G - A_G^T P \\ &- (PB_G + C_G^T)(-\gamma^2 I_{n_d})^{-1}(B_G^T P + C_G), \end{aligned} \tag{20}$$

then γ is an upper bound on the $L_2[0,T]$ to Euclidean gain of G.

Proof. The proof follows the one for Theorem 3.7.4 in Green and Limebeer (1995).

4. FAULT DETECTION SYSTEM DESIGN FOR THE AIRBUS BENCHMARK

The design of a model-based fault detection filter providing fast detection times for small OFC amplitudes and no false alarms features several challenges. Firstly, the aerodynamic force input is unknown, but its direct decoupling is not possible due to only one available measurement. Secondly, uncertain parameters are present which provide a spread in the actuator dynamics. Thirdly, the non-linear function $f_{i_c \to v_c}$ with discontinuities is nested in the model, complicating the actual generation of the detector.

4.1 Actuator Model Approximation

To address these challenges a simplified, non-linear multi-model of the actuator is derived which can be used for the design of a multi-model fault detection filter. Therefore, as proposed in Varga et al. (2011), the fault free actuator behavior is approximated with a simpler model,

$$\dot{\tilde{x}} = \tilde{k}^{\Delta}(x_c, \tilde{x}, \dot{\tilde{x}})(x_c - \tilde{x}), \tag{21}$$

where $\tilde{x}$ and $\dot{\tilde{x}}$ are the estimates of the actuator rod position and its velocity and $\tilde{k}^{\Delta}$ is a non-linear actuator gain. The stochastically distributed parameters ΔP^{Δ} and k_d^{Δ} make the estimation of the actuator position difficult as no direct physical reason for their variation can be modeled in the gain $\tilde{k}^{\Delta}$ of the estimator. For fixed values of ΔP^{Δ} and k_d^{Δ}, however, the actuator gain in (2.1) is constant when the actuator is in standstill and varies during motion, i.e., $\dot{x} \neq 0$. Taking this finding and an approximation of the function $f_{i_c \to v_c}$ into account, a suitable approximation of the gain is found by

$$\tilde{k}^{\Delta}(x_c, \tilde{x}, \dot{\tilde{x}}) = c_0^{\Delta} - c_1^{\Delta}\dot{\tilde{x}}^2 + c_2|\dot{\tilde{x}}|(x_c - \tilde{x}), \tag{22}$$

where the parameters c_0^{Δ}, c_1^{Δ}, and c_2 are constant parameters covering the basic actuator gain, the damping effect and the non-linear mapping $f_{i_c \to v_c}$, respectively. Changing the differential pressure can be covered by changing the basic gain c_0, while a change of k_d^{Δ} can be covered via c_1^{Δ}. The influence of the aerodynamic force on the gain is found to be neglectable. For fixed values of the differential pressure ΔP^{Δ} and the damping coefficient k_d^{Δ} the actuator gain can be approximated by solving optimization problem

$$\min_{c_0,c_1,c_2} \sum_{k=1}^{N} (x(t_k) - \tilde{x}(t_k, c_0, c_1, c_2))^2, \tag{23}$$

i.e., minimizing the sum of squared errors between the rod position x of the actuator model in (2) and the rod position $\tilde{x}$ from the approximation in (21) and (22) over N time steps t_k. An impulse-like load-factor input is selected as excitation signal for the aircraft system. Finally, for different settings of ΔP^{Δ} and k_d^{Δ} different model approximations result resulting in a multi-model approximation of the actuator.

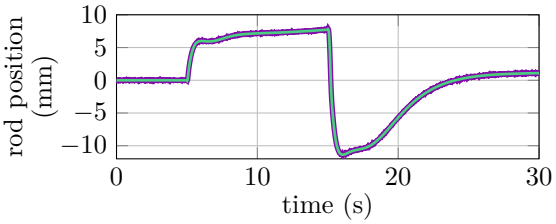

Fig. 1. Measured actuator rod position (——) and its estimate (——) during a load-factor input.

Fig. 1 shows a comparison between the measured rod position x (——) and its approximate $\tilde{x}$ (——) for nominal values of ΔP^{Δ} and k_d^{Δ} during a load-factor step-like input of 0.5 g. The approximation error is considered to be sufficiently small, staying within ±0.2 mm. Note that the worst-case approximation error scales proportionally with the input. Due to the fact that a multi-model approach is used to cover the uncertain parameters k_d^{Δ} and ΔP^{Δ} the error can be keep within ±0.2 mm over the whole parameter range for smaller given inputs than 0.5 g.

4.2 Multi-Model Fault Detection

The basic design conditions for fault detection filters, namely input decoupling and fault coupling, described herein in equations (6) and (7) for linear systems, also hold for non-linear systems. For the non-linear actuator model (21) a valid fault detection filter subtracts the measurement x_m, which get propagated through the inverse actuator model, from the actual input x_c to generate r. As the system in equation (21) is of first order, its inverse requires an additional, arbitrary first order system to make the filter proper. Employing these ideas leads to the non-linear residual filter

$$\begin{aligned}\dot{x}_r &= -ax_r + \begin{bmatrix} a & -\dfrac{a\,(\tilde{k}^{\Delta} - a)}{\tilde{k}^{\Delta}} \end{bmatrix} \begin{bmatrix} x_c \\ x_m \end{bmatrix} \\ r &= x_r + \begin{bmatrix} 0 & -\dfrac{a}{\tilde{k}^{\Delta}} \end{bmatrix} \begin{bmatrix} x_c \\ x_m \end{bmatrix}, \end{aligned} \tag{24}$$

in the time domain, where a is a free parameter defining the filter dynamics. To cover the unknown and uncertain parameters c_0^{Δ} and c_1^{Δ} of the actuator model a bench of filters of the form (24) is derived, enabling the multi-model fault detection approach described in Section 3.1. For each set of different but constant values of c_0^{Δ} and c_1^{Δ} in equation (22) a unique filter is designed. The denser the grid within the known limits of the two parameters is selected, the better the robustness of the fault detection against the uncertainties in these parameters becomes. The decision if an OFC is present or not follows equations (8) and (9). The decision variable i_f is used to trigger the reconfiguration of the FCS.

4.3 Simulation based Verification

The threshold τ in equation (9) is set to 0.94 based on simulation results employing different control inputs, sensor noise and different turbulence levels, see Engelbrecht et al. (2022). The threshold is optimized manually to detect the minimum fault possible while ensuring no false alarms. Further, the threshold value thus directly be interpreted as minimum detectable fault on the rod position in millimeter, which equals a detectable control surface deflection of about $\pm 0.35°$. The free parameter a of the detector (24) has been set to -10, ensuring fast detections.

To verify against false alarms, a fault free analysis has been performed using load-factor step-like-, chirp- inputs, and sine-inputs for different turbulence levels. No false alarms have been detected for load-factor inputs up to ± 0.5 g. For larger inputs, the actuator model approximation shows a bigger error so that the threshold increases adaptively depending on the pilot load-factor command. This ensures no false alarms for inputs up to ± 1.5 g. To verify the detection performance it is assumed the fault occurs the aircraft being in cruise-condition at different turbulence levels. The induced faults are uniformly distributed between 2.5 mA and 30 mA on the current and 2.5 mm and 30 mm on the rod-sensor. The fault frequencies are uniformly distributed between 1 Hz and 10 Hz. In total 1200 simulations have been performed resulting in a missed detection rate of 2.6% and 3.2% late detection rate. All problematic cases correspond to small input amplitudes and high frequencies. As the upper end of the frequency fault spectrum lies below the bandwidth of the actuator the residual is not exceeding an equivalent of $\pm 0.35°$ in control surface deflection.

5. FAULT TOLERANT CONTROL STRATEGY FOR THE AIRBUS BENCHMARK

After an OFC detection two actions are performed in the FCS to meet the requirements defined in Engelbrecht et al. (2022). The control law is reconfigured from the normal to the alternate law and the control allocation is reconfigured to maintain the alternate law's nominal performance. Both actions are performed quickly and smoothly.

5.1 Control Reconfiguration and Reallocation

For the reconfiguration from the normal to the alternate law, the proportional and integral elements of the

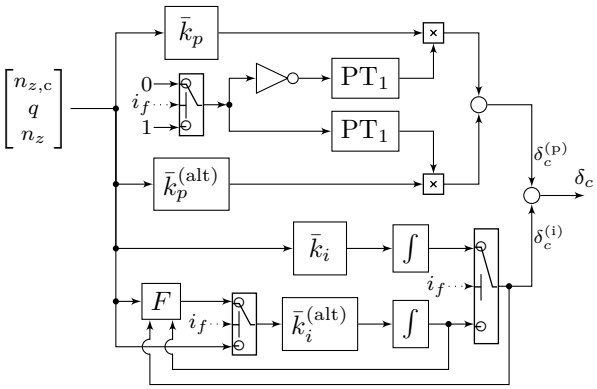

Fig. 2. Illustration of the controller switching scheme.

controllers are separated to enable the hybrid bumpless switching scheme described in Section 3.2. As illustrated in Fig. 2, the proportional gains of the control input are blended using linear proportional first order filters (PT$_1$) according to equation (10) to ramp the new control input up and to fade the old control signal out. The filters' time constant is set to $T = 0.5$ s to meet the allowed 3 s for the reconfiguration process. Note, in Fig. 2 a decision variable $i_f = 0$ means the upper channel of each switch is active, while $i_f = 1$ initiates switches to the lower channels. To ensure a continuous integral contribution during the control law transition the bump-less scheme introduced in Section 3.2 is implemented, indicated by the matrix F from equation (13) in Fig. 2. For determining F via equations (13)-(15) the matrices $\tilde{A} = 0$, $\tilde{B} = \bar{k}_i^{(\mathrm{alt})}$, $\tilde{C} = 1$ and $\tilde{D} = 0_{1\times 3}$ describe the state-space representation of the alternate control law's integral contribution.

In addition, the control allocation needs to be reconfigured to ensure that the alternate law performs as it would with two actuators available. Thus, if an OFC is detected, the contribution of the remaining actuator needs to be doubled, as the faulty actuator is switched off. This is achieved by the simple logic

$$\begin{aligned}\delta_{c,l} &= (1 - i_f)\delta_c \\ \delta_{c,r} &= (1 + i_f)\delta_c, \end{aligned} \tag{25}$$

where $\delta_{c,l}$ and $\delta_{c,r}$ are the commanded deflections on the left and right elevator, respectively.

5.2 Linear Time-Variant System Analysis

For a rapid initial verification of the FTC scheme, an LTV worst-case analysis is performed. The approach avoids time expensive simulation-based analyses in the design phase (see, e.g., Biertümpfel and Pfifer (2022)). The analysis is based on Theorem 1 in Section 3.3. It provides the worst-case upper bound on the flight-path angle γ at the final time T of the considered analysis horizon $[0, T]$ due to a disturbance at the faulty actuator's output.

For the analysis, the closed-loop aircraft system including the linearized actuator dynamics, controller switching, and reallocation scheme is transferred to the LTV framework. The proportional controller blending (10) is modeled by two time-varying gains. For the alternate law path, the value of the gain is 0 before the OFC detection and follows the step response of the first order element afterwards. The nominal law is derived accordingly (from 1 to 0). The bumpless scheme for the integrator is modeled with

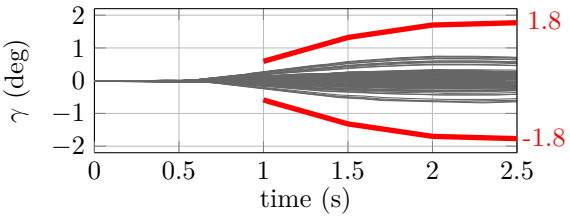

Fig. 3. LTV system analysis bounds on γ (——) compared against non-linear simulation results.

a single integrator with a time-varying gain. The gain's value is $\bar{k}_i$ before and $\bar{k}_i^{(\text{alt})}$ after detection. Two time-varying gains with values according to equation (25) before and after detection model the control reallocation. Based on the results in Section 4.3, the onset time for the reconfiguration is set to 0.5 s. Hence, a maximum analysis horizon up to 2.5 s deems adequate to analyze the reconfiguration.

Theorem 1 only upper bounds γ at the final time T. Hence, the analysis is run for a set of final times $\{1, 1.5, 2, 2.5\}$ s to evaluate the reconfiguration. Moreover, the LTV analysis condition only considers norm bounded inputs with unit energy. This property necessitates the scaling of the disturbance input to calculate interpretable γ values. The $L_2[0, T]$ norm of a solid OFC with a maximum amplitude of 30 mm and 1 Hz defines the disturbance scaling for the respective analysis horizon. These scalings upper bound the norms for the OFC frequency range from 1 Hz to 10 Hz. Fig. 3 depicts the calculated worst-case γ at the end of the time horizons. Values between the analysis grid points are linear interpolated providing a funnel-like worst-case envelope (——). The LTV analysis provides an acceptable, maximum γ-deviation of $\pm 1.8°$ for horizons of 2.5 s. The derived worst-case envelope provides a strict upper bound on 400 non-linear simulations with light turbulence and OFC definitions from Section 4.3.

5.3 Simulation based Verification

To verify the closed-loop performance, a gridded parameter study including different OFC amplitudes, frequencies, and turbulence levels has been performed. As for the detection performance, the analysis involves 1200 runs. Figure 4 depicts the cumulative distributions of the maximum recorded γ in each of the 1200 simulations. For comparison the analysis is performed once without FTC (——) and once using the proposed detection and reconfiguration (——). With FTC algorithms enabled the maximum γ-deviation over all simulation runs is reduced from 4.6° to 2.5°. In both analyses, clearly three clusters are present in the data. They correspond to the three turbulence levels defined in the simulator. The proposed FTC algorithms restrict the γ-deviation to the minimum deviation possible.

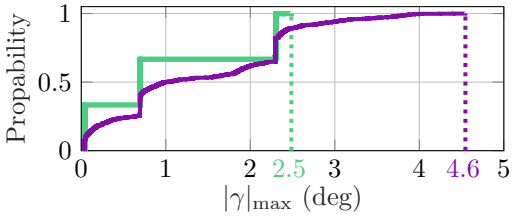

Fig. 4. Maximum flight-path angle cumulative distributions for analysis with (——) and without (——) FTC.

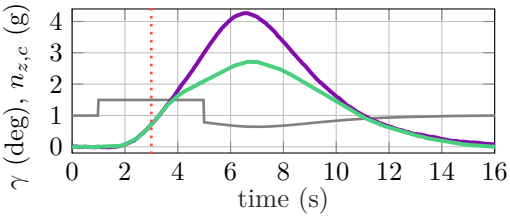

Fig. 5. γ for normal law (——) and reconfiguration scenario (——) during a load-factor input (——).

The remaining deviations are purely driven by the aforementioned turbulence levels. Applying no counteractions during the OFCs leads to a maximum γ-deviation of about 4.6° over all cases. Also, the probability to stay within a certain maximum γ value is strictly higher when using the proposed algorithms, as the corresponding cumulative distribution lies always on or above the distribution when using no counteractions. To verify that no pitch departure occurs regardless when the controller reconfiguration happens, the reconfiguration is initiated during a load-factor step-input maneuver with no OFC is present. Figure 5 compares γ during a step input (——) when using the normal law (——) against a reconfiguration from the normal to the alternate law (——) in the middle of the step input, i.e, at three seconds simulation time. Clearly, no departure from the trim state occurs during the reconfiguration.

REFERENCES

Biertümpfel, F. and Pfifer, H. (2022). Finite horizon analysis of autolanded aircraft in final approach under crosswind. *Control Engineering Practice*, 122, 105105.

Cieslak, J., Henry, D., Zolghadri, A., and Goupil, P. (2008). Development of an active fault-tolerant flight control strategy. *Journal of Guidance, Control, and Dynamics*, 31(1), 135–147.

Cieslak, J., Efimov, D., and Henry, D. (2015). Transient management of a supervisory fault-tolerant control scheme based on dwell-time conditions. *Int. Journal of Adaptive Control and Signal Processing*, 29(1), 123–142.

Engelbrecht, J., Goupil, P., and Oudin, S. (2022). Technical Note describing the joint Airbus-Stellenbosch University Industrial Benchmark on Fault Detection and Fault Tolerant Control. Technical report, IFAC.

Goupil, P. (2010). Oscillatory failure case detection in the A380 electrical flight control system by analytical redundancy. *Control Engineering Practice*, 18, 1110–1119.

Green, M. and Limebeer, D. (1995). *Linear Robust Control*. Information and System Sciences. Prentice Hall, Englewood Cliffs, New Jersey.

Ossmann, D., Joos, H.D., and Goupil, P. (2017). Enhanced Sensor Monitoring to Maintain Optimal Aircraft Handling in Case of Faults. *AIAA Journal of Guidance, Control, and Dynamics*, 40(12), 3127–3137.

Tadmor, G. (1990). Input/output norms in general linear systems. *Int. Journal of Control*, 51(4), 911–921.

Turner, M.C. and Walker, D.J. (2000). Linear quadratic bumpless transfer. *Automatica*, 36(8), 1089–1101.

Varga, A. (2017). *Solving Fault Diagnosis Problems - Linear Synthesis Techniques*. Springer Int. Publishing.

Varga, A., Hecker, S., and Ossmann, D. (2011). Diagnosis of actuator faults using LPV-gain scheduling techniques. In *Proc. of AIAA Guidance, Navigation, and Control Conference*. Portland, Oregon, USA.